Ab initio morphology prediction of Pd, Ag, Au, and Pt nanoparticles on (0001) sapphire substrates

Akio Ishii[1, a)] and Nobutomo Nakamura[2]

[1)] *Department of Mechanical Science and Bioengineering, Osaka University, Osaka 560-8531, Japan*

[2)] *Graduate School of Engineering, Osaka University, 2-1 Yamadaoka, Suita, Osaka 565-0871, Japan*

(Dated: 30 January 2024)

We energetically predict the morphology of Pd, Ag, Au, and Pt nanoparticles on (0001) sapphire substrates, using density functional theory (DFT) simulations and the well-known Young– Dupre equation. In all cases, the contact angles exceed 90°, indicating that the nanoparticles are spherical. Notably, Au nanoparticles exhibit a higher contact angle than those of their counterparts. The validity of the proposed *ab initio* nanoparticle morphology prediction approach based on DFT simulations was assessed in comparison with our previous experimental findings pertaining to the time variation of the full width at half maximum (FWHM) of the resonant peak. Furthermore, the diffusivities of single Pd, Ag, Au, and Pt atoms on the substrate were evaluated by calculating the activation energy, offering insights into the underlying physics governing the timing of FWHM peaks. The analysis confirms a higher diffusivity of Au and Ag compared with Pd and Pt. According to the comparison between DFT and experiment results, although no clear relation is observed between the contact angles and timing of FWHM peaks, the diffusivity of sputtered atoms may influence the timing of FWHM peaks. Thus, the timing can help to clarify the nanoparticle size, rather than the shape.

[a)] Electronic mail: ishii@me.es.osaka-u.ac.jp

I. INTRODUCTION

Nanoparticles exhibit unique properties that differ from those of bulk metals, and extensive research on their properties has been conducted to synthesize them with specific characteristics[1–3]. Previous studies have established that the properties of nanoparticles depend on their size and shape[4–8]. However, accurate experimental investigation of the morphology of these nanoparticles is challenging, especially when synthesized on substrates. In our previous studies, we introduced a novel real-time method based on acoustic techniques for evaluating the morphology[9] and growth of nanoparticles on sapphire substrates[10,11]. We analyzed the morphology of Pd-based core–shell nanoparticles by examining the time-dependent variations in the full width at half maximum (FWHM) of the resonant peak in relation with the surface energy of each species. The shape and internal structure of the core–shell nanoparticles were clarified considering the surface energy of each metal. However, according to the well-known Young–Dupre equation[12], the interfacial effect between nanoparticles also influence the morphology of nanoparticles. Thus, these effects must be considered to gain more comprehensive insights into the morphology.

In this study, to complement our previous research, we used energy principles to predict the morphology of Pd, Ag, Au, and Pt nanoparticles on (0001) sapphire substrates. To this end, density functional theory (DFT) atomistic simulations were performed, incorporating the Young–Dupre equation. The computational results were compared with our previous experimental observations to validate both the previously proposed experimental methods and *ab initio* morphology prediction using DFT simulations, as introduced in this study.

II. METHODOLOGY

The Young–Dupre equation for nanoparticles ($X(= \mathrm{Pd}, \mathrm{Ag}, \mathrm{Au}, \mathrm{Pt})$) on sapphire ($Al_2O_3$) substrates can be expressed as follows:

$$W^{\mathrm{X}-\mathrm{Al_2O_3}} = \gamma^{\mathrm{X}}(1 + \cos\theta). \tag{1}$$

Here, $W^{\mathrm{X}-\mathrm{Al_2O_3}}$ is the adhesion energy between the X nanoparticle and sapphire, and γ^{X} is the surface energy of the nanoparticle. In this study, $W^{\mathrm{X}-\mathrm{Al_2O_3}}$ and γ^{X} were calculated through DFT atomistic simulations, and the contact angle θ was determined to predict the

morphology of X nanoparticle. Each step of the DFT calculation is described in the following subsections.

A. Adhesion energy calculation

The values of the adhesion energy, $W^{\mathrm{X-Al_2O_3}}$, were calculated using potential energy derived from DFT simulations, denoted as E^{X}, $E^{\mathrm{Al_2O_3}}$, and $E^{\mathrm{X-Al_2O_3}}$.

$$W^{\mathrm{X-Al_2O_3}} = \frac{E^{\mathrm{X}} + E^{\mathrm{Al_2O_3}} - E^{\mathrm{X-Al_2O_3}}}{A^{\mathrm{Al_2O_3}}}. \tag{2}$$

Here, $E^{\mathrm{X-Al_2O_3}}$, E^{X}, and $E^{\mathrm{Al_2O_3}}$ represent the interfacial energy between X and sapphire, surface energy of X, and surface energy of sapphire, respectively. $A^{\mathrm{Al_2O_3}}$ denotes the area of the intersurface. Specifically, we calculated E^{X}, $E^{\mathrm{Al_2O_3}}$, and $E^{\mathrm{X-Al_2O_3}}$ using the atomic models shown in Figs. 1 (a), (b), and (c) respectively. In model (a), assuming X(= Pd, Ag, Au and Pt) has a face-centered cubic (FCC) structure, we introduced six (111) X layers (ABCABC... stacking) on the (0001) surface of a 12-layers $\alpha - \mathrm{Al_2O_3}$ sapphire substrate. The numbers of atoms for each species in the model were X=18, Al=24, and O=36. Although several choices are available for the (0001) surface structure of $\alpha - \mathrm{Al_2O_3}$, we selected the most stable structure with the lowest surface energy, with reference to the literature[13]. After constructing the atomic model of the interfacial structure, DFT structural optimization was performed for both the atoms and supercell. The model height was set as 56 nm to introduce vacuum conditions around the surface. Models (b) and (c) were constructed by simply removing the X ($\alpha - \mathrm{Al_2O_3}$) layers from Model (a). $A^{\mathrm{Al_2O_3}}$ was calculated using the cell vectors of the supercell in Model (a).

DFT atomistic simulations were performed using the Vienna Ab initio Simulation Package[14]. The electron–ion interaction was described using the projector-augmented wave method[15]. The exchange-correlation between electrons was treated using the Perdew–Burke–Ernzerhof generalized gradient approximation[16], with an energy cutoff of 520 eV for the plane-wave basis set. Energy convergence criteria for the electronic and ionic structure relaxations were set as 1.0×10^{-6} and 1.0×10^{-3} eV, respectively. A $5 \times 5 \times 1$ k-point mesh was used for all atomic models shown in Fig. 1.

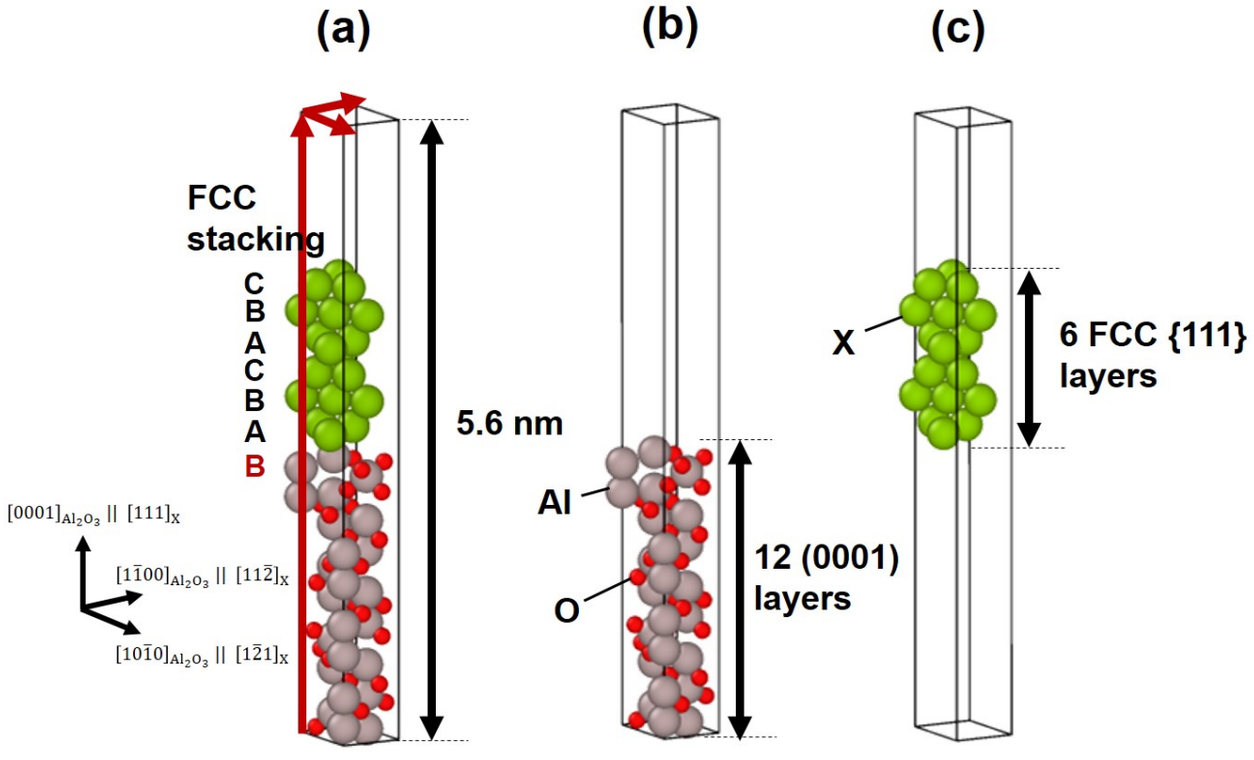

FIG. 1. Atomic models for calculating the adhesion energy $W^{X-Al_2O_3}$, (a) $E^{X-Al_2O_3}$, (b) $E^{Al_2O_3}$, and (c) E^{X}. Red arrows indicate the cell vector of the supercell (black frames) The atomic structures are visualized using the OVITO software[17]

.

B. Surface energy calculation

To calculate the surface energy γ^{X}, we first constructed FCC nanoparticle models for each X using Wulff construction[18,19], implemented using the Atomic Simulation Environment (ASE) Python module[20]. Wulff construction for a certain species can be implemented using the distance d_{ijk} (defined later), yielding polyhedron nanoparticles:

$$d_{ijk} = c\gamma^{\mathrm{X}}_{ijk}. \tag{3}$$

Setting the origin of the coordinate system at the nanoparticle center, we defined planes normal to the $[hkl]$ vectors at a distance d_{hkl} from the origin using known $\gamma^{\mathrm{X}}_{ijk}$ values, representing the surface energy of the plane with the ijk Miller index, and a constant c. In this case, the space within all drawn planes defined the polyhedron of the nanoparticles. The parameter set of $\gamma^{\mathrm{X}}_{ijk}$ for each X is outlined in Table I. By changing the constant c, the nanoparticle size could be modified. As shown in Fig. 2, we constructed four types of nanoparticles with different sizes (number of atoms, n = 55, 79, 141, and 201) for each X species to investigate the change in morphology (θ) with respect to the nanoparticle size. The results indicate that the nanoparticle morphology is independent of the atomic species. The nanoparticles mostly exhibit {111} and {100} surfaces owing to the low energy of {111} surfaces, consistent with the prior research result[21]. However, in the case with 141 atoms, additional {110}, {120}, and {321} surfaces are observed. Following the DFT structural optimization of the constructed nanoparticles, the potential energy of the X nanoparticle E^{Xnp} was calculated. The surface energy γ^{X} was then defined as

$$\gamma^{X} = \frac{E^{\mathrm{Xnp}} - E^{\mathrm{Xbulk}}}{4\pi r^2}. \tag{4}$$

Here, E^{Xbulk} is the potential energy of the bulk FCC structure for X, and r is radius of the nanoparticle, calculated as the circumradius of the nanoparticle polyhedron. For DFT atomistic simulations, a $5.0 \times 5.0 \times 5.0$ nm cubic supercell was used for all nanoparticles to account for the vacuum around the nanoparticles, and a $1 \times 1 \times 1$ k-point mesh was used.

TABLE I. Surface energy for specific orientations (ijk) of the FCC structure of Pd, Ag, Au, Pt, calculated using DFT atomistic simulations, those were derived from the Materials Project database[22]. The unit is J/m^2.

(ijk)	Pd	Ag	Au	Pt
(210)	1.626	0.898	0.906	1.887
(110)	1.574	0.866	0.909	1.681
(211)	1.614	0.868	0.822	1.763
(221)	1.496	0.824	0.780	1.599
(111)	1.339	0.764	0.710	1.488
(332)	1.462	0.793	0.748	1.561
(310)	1.634	0.891	0.906	1.878
(311)	1.570	0.863	0.870	1.791
(331)	1.530	0.852	0.831	1.706
(322)	1.454	0.775	0.748	1.593
(320)	1.637	0.886	0.913	1.894
(321)	1.586	0.861	0.848	1.768
(100)	1.522	0.818	0.861	1.856

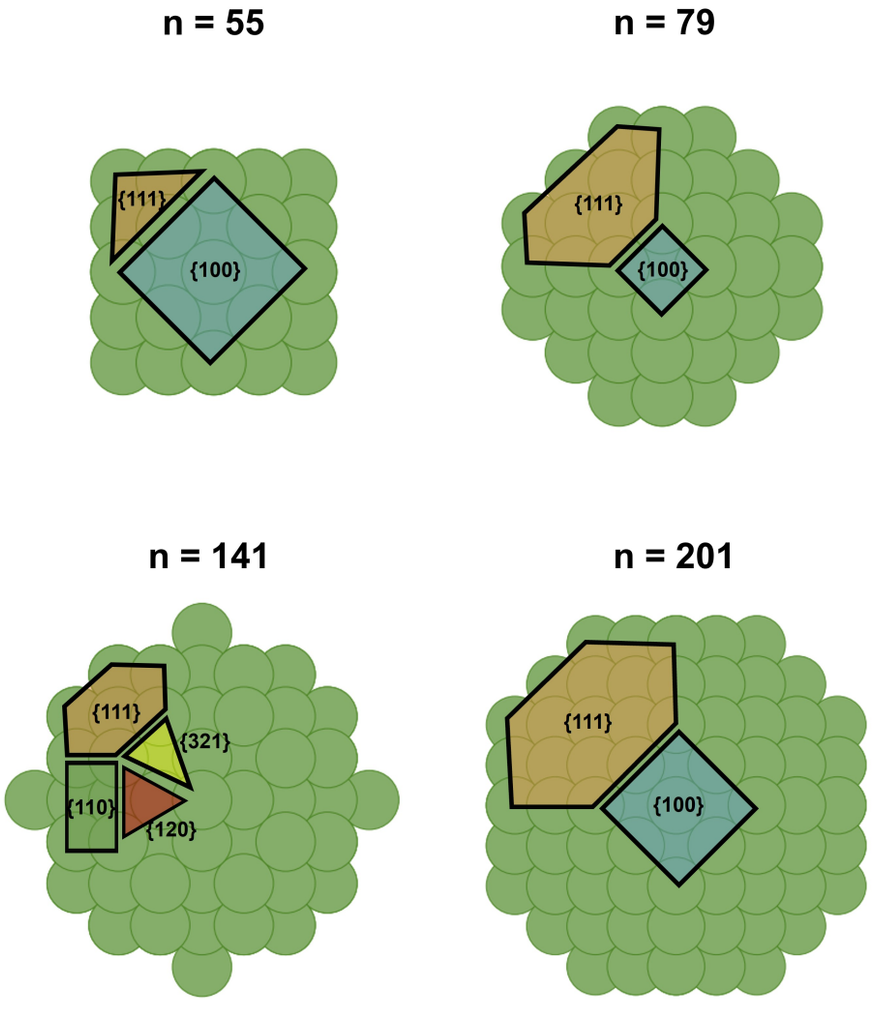

FIG. 2. Atomic models of nanoparticles with different sizes: n =55, 79, 141, and 201 atoms, used for DFT atomistic simulations. All models are constructed using Wulff construction with the surface energy values listed in Table I. The atomic structures of nanoparticles were visualized using the ASE Python module[20]

III. RESULTS AND DISCUSSION

Table II provides the calculated values for E^{X}, $E^{\mathrm{X-Al_2O_3}}$, $A^{\mathrm{Al_2O_3}}$, and $W^{\mathrm{X-Al_2O_3}}$. Notably, $W^{\mathrm{X-Al_2O_3}}$ for Ag and Au are lower than those for Pd and Pt, suggesting a more spherical shape for Ag and Au nanoparticles, as implied by Equation 1. Table III presents the calculated γ^{X} and contact angle θ for each nanoparticle size. For Ag, the calculated surface energy is similar to those reported previously[23–25]. The plots of γ^{X} for different nanoparticle sizes are shown in Fig. 3. The contact angles for all nanoparticles are larger than 90°, indicating their spherical nature. In particular, Au nanoparticles exhibit a higher contact angle compared with other nanoparticles. The spherical nucleation of Ag nanoparticles on Si substrate has been experimentally observed[26]. This outcome is consistent with our result, even though the substrate is different. The difference in contact angle between each species is not substantial, although $W^{\mathrm{X-Al_2O_3}}$ for Ag and Au are lower than those of Pd and Pt. This phenomenon is attributable to the lower surface energy of Ag and Au, resulting in the nanoparticles being flattened on the substrate. Thus, although we discussed the morphology of nanoparticles on the substrate only using the surface energy of nanoparticle in our previous study[11], not only the surface energy, but the interfacial effect between the nanoparticle and substrate are also important; the competition between adhesion energy $W^{\mathrm{X-Al_2O_3}}$ and surface energy γ^{X} is crucial for understanding the morphology of nanoparticles on the substrate, with these values being highly species-dependent.

According to Table III and Fig. 3, the surface energy decreases as the nanoparticle size increases, consistent with findings of prior studies[23–25]. Eventually, as nanoparticles grow, the contact angle decreases, and nanoparticles assume a penny-like flattened shape. This is attributable to the decreasing fraction of edge in the total surface area. For sufficiently large nanoparticles, the effect of edges becomes negligible, and surface energy can be accurately described using only the surface energy of specific Miller index planes, outlined in Table I. Considering the shape of adequately large nanoparticles ($n = \infty$) as truncated octahedrons with (111) hexagons and (100) squares[21], we estimated their surface energy, as indicated in Table III and Fig. 3. Generally, γ^{X} of the smallest nanoparticles ($n = 55$) is 50% larger than that for a nanoparticle with $n = \infty$. Owing to the inherently higher surface energy of Pd and Pt compared with Ag and Au, the edge effect on nanoparticles is more significant for Pd and Pt, resulting in a larger variation in contact angle θ with respect to n, compared with

that for Ag and Au. Through linear interpolation of the plots, we determined that the edge effect becomes negligible at $n = 390$, 470, 440, and 360 for Pd, Ag, Au, and Pt, respectively. Considering that the radius of conventional nanoparticles is larger than 10 nm^2, the edge effect of the nanoparticles may be negligible in such condition.

It is worth mentioning that the shapes of the nanoparticles predicted using Wulff constrcution tends to deviate from the optimal ones if the nanoparticle size is enough small because Wulff construction neglects contributions from edges and vertices and the discrete nature of atomic plane becomes important for the small-size nanoparticles[27]. Actually, in the size range discussed in our study, previous studies reported non-crystalline structures such as icosahedral and decahedral nanoparticles, asymmetric structures and complex structures due to surface reconstruction, that we can not make using Wulff construction, become optimal[28–32]. To discuss this shape effect of nanoparticle to the contact angle, we employed potentitial energy (per atom) of $n = 55$ icosahedral and $n = 144$ decahedral Au nanoparticles from previous DFT calculation, which reported as optimal shapes at the nanoparticle size by Lambie eta al.[30], and use them as E^{Xnp} in equation (4) and re-calculated the contact angle of $n = 55$ and $n = 141$ Au nanoparticles roughly. Note we use the DFT data of $n = 144$ decahedral Au nanoparticle alternatively for $n = 141$ nanoparticle because there is no DFT data of $n = 141$ nanoparticle in Lambie et al.'s literature[30]. The result is 151° for both $n = 55$ and $n = 141$ nanoparticles, which is almost the same as the original values in table I (152°). We think this is because the energy difference between original FCC and optimal complex shapes are not large; only 0.001 eV/atom order (or lower) for Au and Pt though the complex shapes are optimal[30]. Eventually, we concluded the shape effect to the contact angle is not large and negligible.

To validate our *ab initio* morphology prediction, we compared our results with our previous experimental data, specifically, the FWHM timings for Pd, Ag, Au, and Pt. The film thickness vs. FWHM curves for pure Pd, Ag, Au, and Pt atoms, obtained during sputtering onto the sapphire substrate in our previous work[10,11], were re-plotted in Fig. 4. In our previous work, we suggested that the FWHM peak indicates the time at which the nanoparticles of sputtered atoms come into contact. Thus, an earlier (later) appearance of the peak indicates that the nanoparticles on the substrate are flatter (spherical). This interpretation could successfully explain the formation dynamics of core–shell nanoparticles synthesized by sputtering different metals onto nanoparticles[10,11]. Applying this interpretation to the

present results for single -element nanoparticles, Fig. 4 indicates that Pd and Pt nanoparticles may be flatter than Ag and Au nanoparticles, with Ag and Au having higher contact angles. Although the quantitative θ cannot be directly determined from our experimental result, the indication of a higher contact angle of Au nanoparticles compared with Pd and Pt aligns with our prediction. However, the suggestion for Ag nanoparticles contradicts our predictions.

To find the reason of the above contradictions between the calculation and experimental observation, considering that the diffusivity of sputtered atoms onto the substrate also affects the nanoparticle morphology and thus the timing of FWHM peaks[10,11], we investigated the activation energy of the diffusion of single X atoms on a sapphire (0001) surface using the drag method, while detecting the minimum energy path (MEP)[33]. One X atom was placed at the FCC A stacking position on the surface of the Model (b) unit cell shown in Fig. 1. The energy change induced by the movement of the X atom from the initial to final A stacking position along the MEP was calculated to estimate the activation energy of diffusion. The initial estimates for the diffusion path of X atom were obtained through linear interpolation between the initial and final A positions, and nine atomic models of intermediate states were produced with equal intervals along the path for the drag method. Details of the energy and atomic structure changes along the path can be found in the Appendix and supplementary movie. The activation energies are calculated to be 0.20, 0.098, 0.055, and 0.37 eV for Pd, Ag, Au, and Pt, respectively. Compared with those of Pd and Pt atom, the activation energy values for the diffusion of Au and Ag atoms is low (less than 0.1 eV), indicating that these atoms can move more freely on the sapphire surface without significant thermal obstacles. This finding is qualitatively consistent with the timing of FWHM peaks shown in Fig. 4. The atomic diffusion process of sputtered atoms on the surface are well captured by the FWHM peaks: A faster surface diffusion results in a later timing of the peak. In this context, we argue that the size of nanoparticles can be discussed using our FWHM peaks. Small nanoparticles grow separately owing to the high activation energy of diffusion for Pd and Pt sputtering, resulting in the earlier appearance of FWHM peak. In contrast, atoms gather to form one large nanoparticle for Ag and Au sputtering, reducing the surface energy and delaying the timing of FWHM peaks. To confirm this interpretation, we investigated the size of nanoparticles resulting from experimental Pd and Au sputtering using scanning electron microscopy (SEM). The SEM images shown in Fig. 5 reveal large Au nanoparticles,

whereas the Pd nanoparticles are small.

TABLE II. Calculated E^{X}, $E^{\mathrm{X-Al_2O_3}}$, $A^{\mathrm{Al_2O_3}}$, and $W^{\mathrm{X-Al_2O_3}}$. The units are eV for E^{X}, $E^{\mathrm{Al_2O_3}}$, and $E^{\mathrm{X-Al_2O_3}}$; nm^2 for $A^{\mathrm{Al_2O_3}}$; and J/m^2 for $W^{\mathrm{X-Al_2O_3}}$.

X	E^{X}	$E^{\mathrm{Al_2O_3}}$	$E^{\mathrm{X-Al_2O_3}}$	$A^{\mathrm{Al_2O_3}}$	$W^{\mathrm{X-Al_2O_3}}$
Pd	-90.46	-445.08	-536.55	0.2014	0.806
Ag	-46.56	-444.99	-491.93	0.2057	0.300
Au	-55.96	-445.06	-501.20	0.2041	0.138
Pt	-106.13	-445.06	-551.98	0.2009	0.632

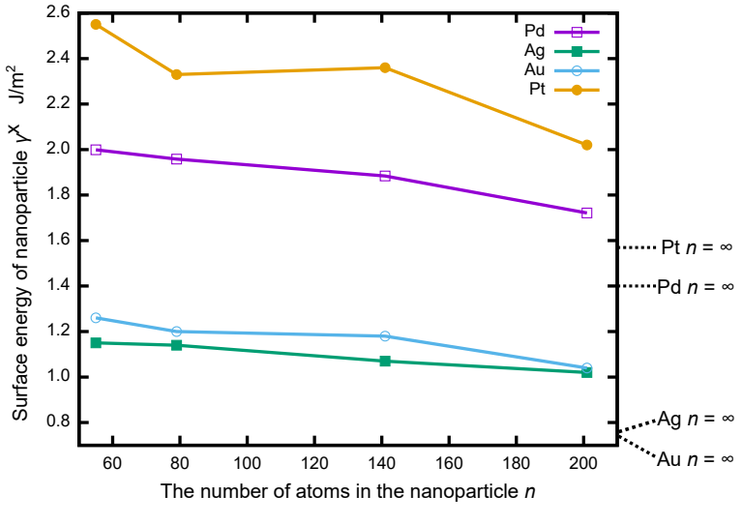

FIG. 3. Change in the surface energy of nanoparticles, γ^{X}, with the number of atoms in the nanoparticle, n.

TABLE III. Calculated γ^{X} and contact angle θ for each nanoparticle size. The units of γ^{X} and θ are J/m^2 and $^\circ$, respectively. Here, $n = \infty$ nanoparticles represent truncated octahedrons with (111) hexagons and (100) squares *without* edge effects.

X	n	γ^{X}	θ
Pd	55	2.00	127
	79	1.95	126
	141	1.88	125
	201	1.72	122
	∞	1.40	115
Ag	55	1.15	138
	79	1.14	138
	141	1.07	136
	201	1.01	135
	∞	0.77	128
Au	55	1.26	152
	79	1.20	152
	141	1.18	152
	201	1.05	150
	∞	0.74	144
Pt	55	2.55	139
	79	2.34	136
	141	2.36	137
	201	2.02	133
	∞	1.57	126

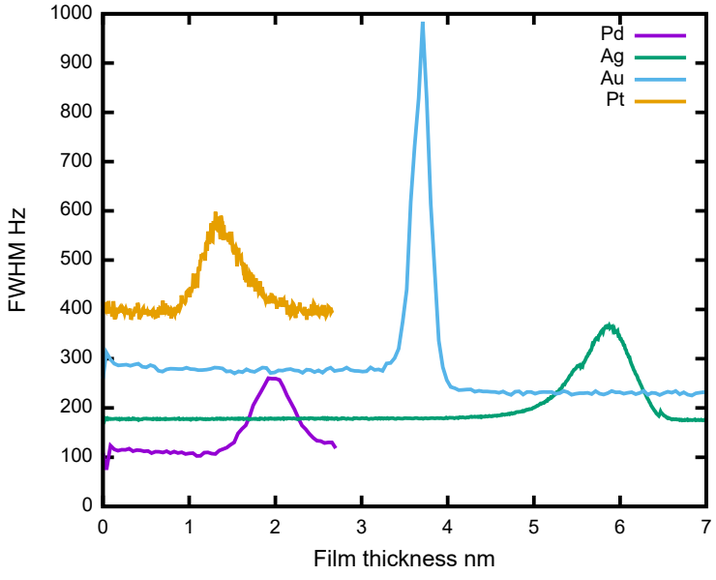

FIG. 4. Change in FWHM during sputtering of pure Pd, Ag, Au, and Pd atoms onto a sapphire substrate. The data are extracted from our previous work[11].

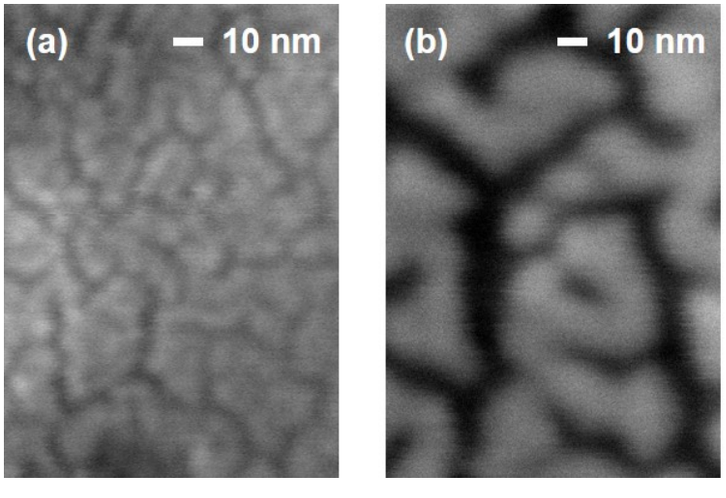

FIG. 5. SEM images showing the morphology of (a) Pd and (b) Au nanoparticles on a sapphire substrate.

IV. SUMMARY

This paper proposes a novel strategy for the morphology prediction of Pd, Ag, Au, and Pt nanoparticles on (0001) sapphire substrates, based on DFT simulations and the well-known Young–Dupre equation. For all nanoparticles, the contact angles are larger than 90°, indicating their spherical nature. Notably, Au nanoparticles demonstrate a higher contact angle compared with the other metal nanoparticles. As the nanoparticle size increases, the contact angles decrease, leading to a more penny-like shape on the substrates. The validity of the proposed *ab initio* morphology prediction of method is demonstrated through a comparison with previous experimental results. The diffusivities of single Pd, Ag, Au, and Pt atoms on the substrate are evaluated by calculating the activation energy to discuss the inherent physics governing the timing of FWHM peaks. The results demonstrate the higher diffusivity of Au and Ag compared with that of Pd and Pt. From the comparison of DFT and experiment result, although there appears to be no significant correlation between the contact angles and timing of FWHM peaks, the diffusivity of sputtered atoms may indeed be linked to the timing of FWHM peaks. The timing can likely provide insights into the size of the nanoparticles rather than the shape. The proposed method is applicable for the morphology prediction of nanoparticles on other types of substrates, such as silicon, as well as for predicting the morphologies of core–shell nanoparticles. These aspects will be considered in future work .

APPENDIX

The calculated changes in the potential energy and atomic structure along the minimum energy path (MEP) for the surface diffusion of an X atom (X= Pd, Ag, Au, Pt) on a sapphire (0001) substrate are shown in Fig. 6. The asymmetrical shape of the potential energy changes with respect to the middle reaction coordinate (denoted as 5) is because the Al atoms around X atoms are not all on the same (0001) plane in the α–Al_2O_3 structure: There are certain deviations in position along the [0001] direction between them. Notably, the atomic structure changes along the MEP do not exhibit significant dependence on the X species, consistent with the observations in our supplementary movie. Conversely, the shape of the potential energy surface for diffusion appears to vary with the species. Notably, Pt exhibits a local minimum at the middle reaction coordinate 5, and the stable state for Ag atoms differs from that of other species, occurring at reaction coordinate 8. Because the investigation into the underlying reasons for these species-specific variations is not the primary focus of this study, we refrain from delving into further discussion.

SUPPLEMENTARY MATERIAL

Supplementary movie of the atomic structure changes along the MEP for the surface diffusion of an X atom on a sapphire (0001) substrate, which we explained in the appendix section above, is available.

ACKNOWLEDGMENTS

This study was partially supported by JSPS KAKENHI Grant Number JP21K03771. The authors would like to thank Koji Matsuura for his technical assistance.

AUTHOR DECLARATIONS

Conflict of Interest

The authors have no conflicts to disclose.

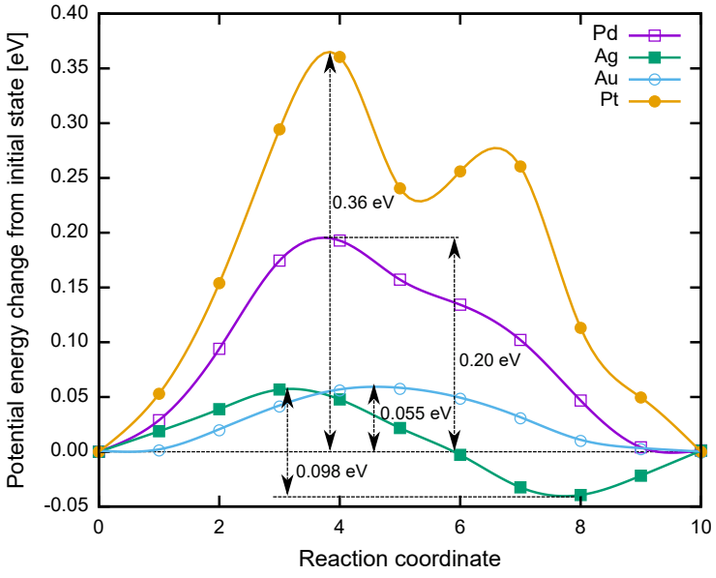

FIG. 6. Potential energy changes for the diffusion of an X atom (X= Pd, Ag, Au, Pt) on sapphire (0001) surface. Reaction coordinates 0 and 10 indicate the initial and final states of the drag method (both correspond to positions of the FCC A stacking atoms in Fig. 2). The curves in the figure serve as visual guides. The changes in the atomic structure along the MEP of diffusion are shown in a supplementary movie.

Author Contributions

A. Ishii: Conceptualization (lead); Formal analysis (equal); Funding acquisition (lead); Investigation (equal); Methodology (lead); Software (lead); Writing-original draft (lead); Writing-review and editing (equal). N. Nakamura: Formal analysis (equal); Investigation (equal); experiment (lead); Writing-original draft (supporting); Writing-review and editing (equal).

DATA AVAILABILITY

The data that support the findings of this study are available from the corresponding author upon reasonable request.

REFERENCES

[1]C. M. Welch and R. G. Compton, "The use of nanoparticles in electroanalysis: a review," Anal. Bioanal. Chem. **384**, 601–619 (2006).

[2]V. Mohanraj and Chen, "Nanoparticles-a review," Trop. J. pharm.l res. **5**, 561–573 (2006).

[3]R. Ferrando, J. Jellinek, and R. L. Johnston, "Nanoalloys: From theory to applications of alloy clusters and nanoparticles," Chem. Revi. **108**, 845–910 (2008).

[4]H. R. Stuart and D. G. Hall, "Island size effects in nanoparticle-enhanced photodetectors," Appl. Phys. Lett. **73**, 3815–3817 (1998).

[5]R. Narayanan and M. A. El-Sayed, "Catalysis with Transition Metal Nanoparticles in Colloidal Solution: Nanoparticle Shape Dependence and Stability," J. Phys. Chem. B **109**, 12663–12676 (2005).

[6]A. Albanese, P. S. Tang, and W. C. Chan, "The Effect of Nanoparticle Size, Shape, and Surface Chemistry on Biological Systems," Annual Rev. Biomed. Eng. **14**, 1–16 (2012).

[7]X. H. Liu, L. Zhong, S. Huang, S. X. Mao, T. Zhu, and J. Y. Huang, "Size-Dependent Fracture of Silicon Nanoparticles During Lithiation," ACS Nano **6**, 1522–1531 (2012).

[8]J. Zheng, C. Zhou, M. Yu, and J. Liu, "Different sized luminescent gold nanoparticles," Nanoscale **4**, 4073 (2012).

[9]N. Nakamura and H. Ogi, "Resistive spectroscopy coupled with non-contacting oscillator for detecting discontinuous-continuous transition of metallic films," Appl. Phys. Lett. **111**, 101902 (2017).

[10]N. Nakamura, K. Matsuura, A. Ishii, and H. Ogi, "Restructuring in bimetallic core-shell nanoparticles: Real-time observation," Phys. Rev. B **105**, 125401 (2022).

[11]N. Nakamura, K. Matsuura, and A. Ishii, "In situ observation of morphological change of Pd-based bimetallic nanoparticles synthesized by co-sputtering," J. Appl. Phys. **134**, 145301 (2023).

[12]R. A. Swalin, *Thermodynamics of solids* (John Wily & Sons, Inc., 1963).

[13]J. Guo, H. L. Chang, and D. J. Lam, "Substrate surface step effects on microstructure of epitaxial films," Appl. Phys. Lett. **61**, 3116–3117 (1992).

[14]G. Kresse and J. Furthmüller, "Efficient iterative schemes for ab initio total-energy calculations using a plane-wave basis set." Physi. Rev. B **54**, 11169–11186 (1996).

[15]G. Kresse and D. Joubert, "From ultrasoft pseudopotentials to the projector augmented-wave method," Phys. Rev. B **59**, 11–19 (1999).

[16]J. Perdew, K. Burke, and M. Ernzerhof, "Generalized Gradient Approximation Made Simple," Phys. Rev. Lett. **77**, 3865–3868 (1996).

[17]A. Stukowski, "Visualization and analysis of atomistic simulation data with OVITO?the Open Visualization Tool," Modell. Sim.Mater. Sci. Eng. **18**, 015012 (2010).

[18]G. Wulff, "Xxv. zur frage der geschwindigkeit des wachsthums und der auflösung der krystallflächen," Z. Kristall. **34**, 449–530 (1901).

[19]G. D. Barmparis, Z. Lodziana, N. Lopez, and I. N. Remediakis, "Nanoparticle shapes by using Wulff constructions and first-principles calculations," Beil. J. Nanotech. **6**, 361–368 (2015).

[20]A. Hjorth Larsen, J. JØrgen Mortensen, J. Blomqvist, I. E. Castelli, R. Christensen, M. Dułak, J. Friis, M. N. Groves, B. Hammer, C. Hargus, E. D. Hermes, P. C. Jennings, P. Bjerre Jensen, J. Kermode, J. R. Kitchin, E. Leonhard Kolsbjerg, J. Kubal, K. Kaasbjerg, S. Lysgaard, J. Bergmann Maronsson, T. Maxson, T. Olsen, L. Pastewka, A. Peterson, C. Rostgaard, J. SchiØtz, O. Schütt, M. Strange, K. S. Thygesen, T. Vegge, L. Vilhelmsen, M. Walter, Z. Zeng, and K. W. Jacobsen, "The atomic simulation environment - A Python library for working with atoms," J. Phys. Cond. Matter **29**, 273002 (2017).

[21]S. Divi and A. Chatterjee, "Generalized nano-thermodynamic model for capturing size-dependent surface segregation in multi-metal alloy nanoparticles," RSC Advances **8**, 10409–10424 (2018).

[22]A. Jain, S. P. Ong, G. Hautier, W. Chen, W. D. Richards, S. Dacek, S. Cholia, D. Gunter, D. Skinner, G. Ceder, *et al.*, "Commentary: The materials project: A materials genome approach to accelerating materials innovation," APL mater. **1**, 011002 (2013).

[23]K. K. Nanda, A. Maisels, F. E. Kruis, H. Fissan, and S. Stappert, "Higher Surface Energy of Free Nanoparticles," Phys. Rev. Lett. **91**, 106102 (2003).

[24]K. K. Nanda, A. Maisels, F. E. Kruis, H. Fissan, and S. Stappert, "Nanda et al. Reply:," Phys. Rev. Lett. **92**, 179602 (2004).

[25]B. Medasani, Y. H. Park, and I. Vasiliev, "Theoretical study of the surface energy, stress, and lattice contraction of silver nanoparticles," Phys. Rev. B **75**, 235436 (2007).

[26]T. W. Oates, H. Sugime, and S. Noda, "Combinatorial surface-enhanced raman spectroscopy and spectroscopic ellipsometry of silver Island films," J. Phys. Chem. C **113**, 4820–4828 (2009).

[27]F. Baletto, R. Ferrando, A. Fortunelli, F. Montalenti, and C. Mottet, "Crossover among structural motifs in transition and noble-metal clusters," J. Chem. Phys. **116**, 3856–3863 (2002).

[28]M. Settem, R. Ferrando, and A. Giacomello, "Tempering of Au nanoclusters: Capturing the temperature-dependent competition among structural motifs," Nanoscale **14**, 939–952 (2022).

[29]M. Settem, C. Roncaglia, R. Ferrando, and A. Giacomello, "Structural transformations in Cu, Ag, and Au metal nanoclusters," J. Chem. Phys. **159**, 094303 (2023).

[30]S. G. Lambie, G. R. Weal, C. E. Blackmore, R. E. Palmer, and A. L. Garden, "Contrasting motif preferences of platinum and gold nanoclusters between 55 and 309 atoms," Nanoscale Advances **1**, 2416–2425 (2019).

[31]H. Xu, M. Molayem, and M. Springborg, "Theoretical study of the structural and energetic properties of platinum clusters with up to 60 atoms," Str. Chem. **32**, 469–479 (2021).

[32]D. Nelli, "Central vacancy creation in icosahedral nanoparticles induced by the displacement of large impurities," Eur. Phys. J. Appl. Phys. **97**, 18 (2022).

[33]H. Jonsson, G. Mills, and K. W. Jacobsen, "Nudged elastic band method for finding minimum energy paths of transitions, in: B.j. berne, g. ciccotti, d.f. coker (eds.), classical," in *Classical and Quantum Dynamics In Condensed Phase Simulations* (World Scientific, Singapore, 1998).